

# Design and Implementation of an Optical Cavity Locking Controller Test Bed System

Abhijit G. Kallapur, *Member, IEEE*, Dirk Schütte, Ian R. Petersen, *Fellow, IEEE*,  
 Toby K. Boyson, *Member, IEEE*, Elanor Huntington, *Member, IEEE*,  
 Sayed Z. Sayed Hassen, *Member, IEEE*, Hongbin Song, and Michèle Heurs

**Abstract**—This paper describes a new optical cavity controller test bed system for implementing modern quantum control techniques, with an emphasis on the control of optical cavities. One such quantum control task is the frequency locking of an optical cavity. Locking an optical cavity refers to the process of matching the input laser frequency to the cavity's resonant frequency. Any deviation in the two frequencies, characterized in terms of the detuning, is undesirable. The test bed comprises an input laser, a three-mirror ring cavity, the associated optics, and a dSPACE digital signal processing system. The detuning in the system is measured in the form of an error signal, which is fed to a controller. The controller provides a suitable control input to a piezoelectric actuator mounted on one of the mirrors, altering the resonant frequency of the cavity to achieve zero detuning. The dynamics of the cavity and the piezoelectric actuator are modeled using system identification methods, an integral linear quadratic Gaussian controller is designed and implemented in dSPACE, and experimental results are presented.

**Index Terms**—dSPACE, frequency locking, frequency response, linear quadratic Gaussian control, optical cavity, system identification.

## I. INTRODUCTION

TECHNOLOGICAL advances over the past few decades have aided in bridging the gap between quantum theory and corresponding experimental results using quantum optics. An important part of this research has been made possible by the application and implementation of feedback control techniques in frequency locking optical cavities. Some of the applications of cavity locking include gravitational-wave interferometry [1], [2], frequency stabilization of semiconductor lasers [3], cavity-enhanced spectroscopic techniques [4], [5], cavity quantum electrodynamics [6], microcavities [7], [8], as well as in general atomic, molecular, and optical physics [9].

Optical cavities, in their simplest form, consist of two mirrors, which can be enclosed, in vacuum cavities, or can

Manuscript received October 22, 2013; revised March 31, 2014; accepted June 6, 2014. Date of publication July 14, 2014; date of current version February 11, 2015. Manuscript received in final form June 12, 2014. This work was supported by the Australian Research Council. Recommended by Associate Editor G. Cherubini.

A. G. Kallapur, I. R. Petersen, T. K. Boyson, E. Huntington, and H. Song are with the School of Engineering and Information Technology, Australian Defence Force Academy, University of New South Wales, Canberra, ACT 2600, Australia (e-mail: abhijit.kallapur@gmail.com; i.r.petersen@gmail.com; t.boyson@adfa.edu.au; e.huntington@adfa.edu.au; h.song@adfa.edu.au).

D. Schütte and M. Heurs are with the Centre for Quantum Engineering and Space-Time Research, Leibniz Universität Hannover 30167, Germany (e-mail: dirk.schuette@aei.mpg.de; michele.heurs@aei.mpg.de).

S. Z. S. Hassen is with the Department of Electrical and Electronic Engineering, University of Mauritius, Moka, Mauritius (e-mail: sayed.hassen@gmail.com).

Color versions of one or more of the figures in this paper are available online at <http://ieeexplore.ieee.org>.

Digital Object Identifier 10.1109/TCST.2014.2331274

be designed to operate in open air. It is required to maintain a frequency lock between the input laser frequency and resonant frequency of the cavity, to achieve constructive interference in order to build maximum energy inside the cavity. Any deviation from the locking frequency is undesirable and is characterized in terms of the detuning parameter  $\Delta$ . Frequency locking ( $\Delta = 0$ ) can be achieved by altering the distance between the mirrors of the cavity, hence modifying its resonant frequency. One way of experimentally realizing this is by controlling a piezoelectric transducer (PZT) mounted on one of the mirrors. Traditionally, cavity locking has been achieved using analog proportional-integral-derivative (PID) controllers and optical techniques [2], [10]–[13].

The idea of applying systematic modern control techniques to quantum optics experiments has been of interest over the past decade, especially in light of recent theoretical developments in extending ideas of classical control systems theory to applications involving quantum systems [14]–[17]. In order to effectively apply a variety of modern control techniques to the problem of locking an optical cavity, we have implemented a standardized, reconfigurable experimental setup, where the measurements are directly related to quantum optical control models of the closed-loop system. The experimental test bed used in this brief comprises of two subsystems: 1) a standard, well-known, and stable optical cavity with associated laser and optics, the properties of which are measured using the quantum optical standard method of homodyne measurements and 2) a reconfigurable digital control setup comprising of a dSPACE digital signal processing (DSP) system to design and implement modern controllers.

There are two key aspects to the optical side of the experimental setup used in this brief. First, the use of a well-known three-mirror optical ring cavity. Second, the use of the homodyne error measurement scheme. The particular three-mirror cavity used here is commonly used in the literature for building cavities in quantum optical applications, and is specifically known as the premode cleaner. Such a cavity was originally proposed in [18] in order to provide the laser requirements for the laser interferometer gravitational wave observatory [1]. It has become close to the industry standard in quantum optics experiments due to its spatial and temporal laser filtering characteristics as well as its inherent stability (see [18]) when compared with other set ups used in the literature, such as [19].

The homodyne method [20], for measuring an error signal, or frequency discriminator, has been chosen for this test bed. Many techniques have been used to extract an error signal in cavity-locking experiments, including the fringe-side

method [21], dither method [22], [23], Pound–Drever–Hall method [24], [25], and Pound/Hänsch method [26]. The homodyne method was chosen because it is the only technique that is based on a direct measurement of a quantum optical observable of the optical cavity. Thus, the homodyne method is the only one that allows measurement results to be incorporated directly into a fully quantum optical description of the control system as required for the implementation of systematic quantum control techniques.

As a first step in designing an integral linear quadratic Gaussian (LQG) controller, we identify a model for the three-mirror ring cavity system. There are many ways to obtain a model for an optical cavity. One of these methods is to begin with the annihilation-creation framework from quantum physics and rewrite it in the form of phase and amplitude quadratures [27], [28]. In general, it is difficult to estimate the parameters involved in such a model as they change from one experimental setup to another. In order to circumvent this issue, we conduct a frequency response analysis for the cavity system in order to obtain a suitable model. Frequency response data for the plant (cavity and PZT actuator) is recorded using a digital signal analyzer (DSA). This data is truncated for the purpose of controller design to include only the first resonance of the system and a state-space model is generated using the frequency domain prediction error minimization (PEM) [29] method in the MATLAB system identification toolbox. Such data truncation is justified by the fact that it is usually only necessary to suppress the first resonant mode, which is the primary mode of the cavity and contributes the most to the motion in the cavity system. In addition, this mode is generally the most affected by environmental noise and input harmonics [30], [31]. One of the two outputs of the cavity is sensed using a homodyne detection scheme, which provides an error signal to the controller. This error signal is proportional to the detuning in the system and the control objective is to reduce the detuning to zero. This error signal is augmented with an integrator in order to provide rejection of low-frequency disturbances, reduce the overall sensitivity to model errors at low frequencies, and provide robust closed-loop performance in the presence of drift in the homodyne error signal. This augmentation of an integrator stage at the output of the plant leads to two signals at the input to the integral LQG controller. This controller is implemented using a dSPACE DSP system. Although the test bed is designed to provide a platform to test a range of modern control techniques, other schemes such as  $H_\infty$  control, model predictive control, and extremum seeking control, are not within the scope of the current paper and may be considered as part of future work. A preliminary version of this paper was presented at the 2012 IEEE Multiconference on Systems and Control [32].

The main contributions of this brief are: 1) the design and implementation of a benchmark optical cavity controller test bed system and 2) the design and implementation of an integral LQG controller for locking the optical cavity in this test bed system, including experimental results.

## II. OPTICAL CAVITY CONTROLLER TEST BED SYSTEM

A schematic of the optical cavity controller test bed system is depicted in Fig. 1. The optical cavity in the test bed

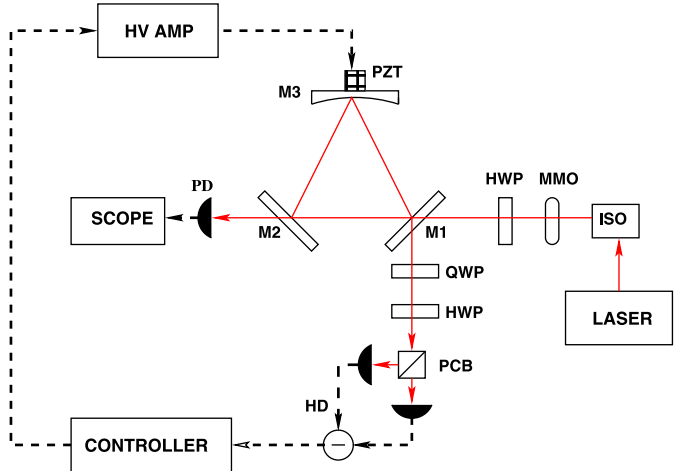


Fig. 1. Block diagram of the cavity locking controller test bed system. The solid lines indicate optical signal paths and the dashed lines represent electrical signal paths.

system is an open air cavity comprising of three mirrors M1, M2, and M3, which are arranged in a ring fashion. Mirrors M1 and M2 are both partially reflecting (with reflectivity  $R = 97\%$ ) and are rigidly mounted on an optical table. A PZT actuator is mounted on mirror M3 ( $R = 99.9\%$ ), which is used to alter the distance between the mirrors, effectively changing the resonant frequency of the cavity. Light from a fiber-coupled 1550-nm diode laser (LASER) is passed through a fiber isolator (ISO) before being coupled into free space through a collimator. The beam passes through mode matching optics to couple efficiently into the cavity, defined by mirrors M1, M2, and M3. The reflected beam is measured using the homodyne error measurement technique.

As mentioned in Section I, the homodyne measurement technique was chosen to make the test bed mathematically amenable to systematic quantum control techniques. To illustrate this point, consider the quantum optical model for a three-mirror cavity [27], [28]

$$\begin{aligned} \dot{a} &= -(\kappa + i\Delta)a + \sqrt{2\kappa_1}A_{in} + \sqrt{2\kappa_2}\delta A_v + \sqrt{2\kappa_3}\delta A_t \\ A_r &= \sqrt{2\kappa_1}a - A_{in} \\ A_t &= \sqrt{2\kappa_2}a - \delta A_v. \end{aligned} \quad (1)$$

Here,  $a$  denotes the annihilation operator for the cavity mode defined in an appropriate rotating frame. The detuning  $\Delta$  represents the frequency deviation of the cavity's resonant frequency from the nominal laser frequency  $\omega_0$ . The cavity decay rates  $\kappa_i$  are determined by mirror reflectivities  $R_i$  and are given by  $\kappa_i = (1-R_i)/2\tau$  for a cavity round-trip time of  $\tau$ . The total decay rate is given by  $\kappa = \kappa_1 + \kappa_2 + \kappa_3$ . In addition,  $\delta A_t$  is the vacuum noise entering mirror M3 and  $\delta A_v$  is the vacuum noise entering mirror M2.  $A_{in}$  is the input laser field,  $A_r$  is the reflected optical field at M1, which is used by the homodyne detector (HD), and  $A_t$  is the transmitted optical field at mirror M2 detected by the photodetector (PD) in Fig. 1.

Here, we have assumed that all loss in the optical cavity arises from mirror M3. In quantum optics, the vacuum field is treated as having zero mean but nonzero fluctuations. Therefore, the quantum optical model for the cavity must incorporate vacuum fields impinging on the cavity through

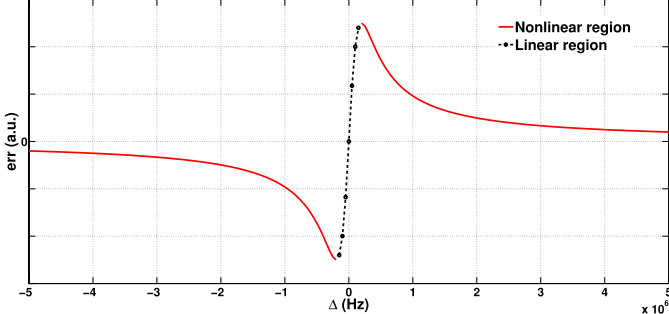


Fig. 2. Variation of the error signal (output of the HD) with the detuning parameter  $\Delta$ . Here, arbitrary units are abbreviated as a.u.

mirrors M2 and M3 (driven by  $\delta A_v$  and  $\delta A_l$ , respectively) in addition to incorporating the driving field incident on the front face of the cavity as given by  $A_{in}$ . The field transmitted through the cavity is given by  $A_t$  and the reflected field is  $A_r$ .

The annihilation operator is not an observable (i.e., it cannot be measured) of a quantum optical field. However, the amplitude and phase quadratures are observables and are denoted  $X_i^+ = A_i + A_i^\dagger$  and  $X_i^- = iA_i - iA_i^\dagger$ , respectively, where  $A_i^\dagger$  is the Hermitian conjugate of  $A_i$ . From these definitions, it is possible to construct a state-space model of the quantum optical cavity, which incorporates quantum-optically allowed measurements (such as  $X_r^-$ , the phase quadrature of the reflected field) as well as models of the dynamics of the classical components of the system (such as mirror position) through the dynamics for the detuning  $\Delta$ .

The intracavity annihilation operator can be decomposed into  $a = \langle a \rangle + \delta a$  as can the input  $A_{in} = \langle A_{in} \rangle + \delta A_{in}$ . By definition, the vacuum inputs have  $\langle A_l \rangle = \langle A_v \rangle = 0$  and we set  $\Delta = \langle \Delta \rangle + \delta \Delta = \bar{\Delta} + \delta \Delta$ . Under such circumstances, (1) can be solved in steady-state to find that

$$X_r^\pm = \frac{2\kappa_1}{\kappa^2 + \bar{\Delta}^2} (\kappa X_{in}^\pm \mp \bar{\Delta} X_{in}^\mp) - X_{in}^\pm. \quad (2)$$

From here on, we will assume without loss of generality that the input field is real (i.e.,  $X_{in}^- = 0$ ), effectively setting the input field to be the phase reference for the experiment. Fig. 2 shows a plot of (2). Linearizing (2) near  $\Delta = 0$ , we find that steady-state measurements of the phase quadrature of the output field are linearly proportional to the detuning  $\Delta$  and hence can be used as an error signal. This is the key observation underpinning the application of homodyne measurements to the control problem of cavity locking.

Quantum optical homodyne measurement requires that a strong, phase-coherent optical local oscillator interferes with the field of interest with difference detection of the two fields resulting from the optical interference process [28]. The relative phase between the two fields determines which quadrature of the field of interest is measured, with a  $\pi/2$  relative phase being required to measure the phase quadrature. To avoid the need for complicated techniques to control and match the local oscillator to the fields that interact with the optical cavity, the homodyne method [20] makes use of a local oscillator that copropagates with the field to be measured but which is in an orthogonal polarization. Homodyne measurement of the phase

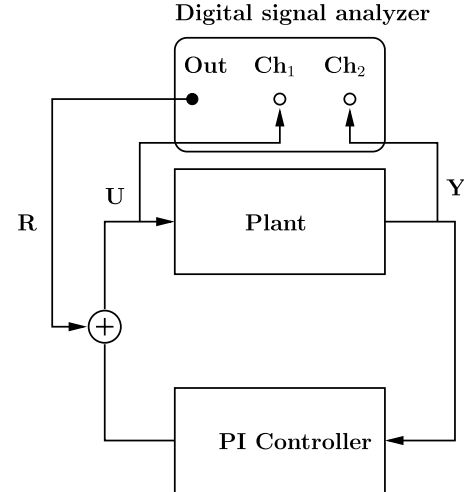


Fig. 3. DSA setup used to obtain frequency response data for the plant (cavity and piezoelectric actuator).

quadrature of the reflected beam is implemented by passing the reflected beam through a quarter-wave plate and a half-wave plate, which together introduce the requisite relative phase shift  $\pi/2$  phase shift, before being split with a polarizing cube beamsplitter, which yields the two interfered output fields, and then detected by HD, which comprises two PDs followed by subtraction electronics. The output of the HD is directly proportional to the phase quadrature of the quantum optical field reflected from the optical cavity. The output of the HD, often called the error signal, is sent to a controller (CONTROLLER) implemented on a DS1104 dSPACE DSP board. The output of the controller is amplified using a  $\pm 200$  V high voltage amplifier (HV AMP) to drive a PZT actuator mounted on mirror M3. Transmitted light from the cavity is monitored using a PD and a Rigol SD1052E digital oscilloscope (SCOPE). The PDs were designed and built as outlined in [33]. Both the detectors, and the high voltage amplifier, were designed and built at UNSW Canberra.

The control objective is to regulate the detuning  $\Delta$  to zero, which corresponds to driving the error signal (output of the HD) to zero, while maintaining the transmitted signal (output of mirror M2) at a maximum. This ensures that the cavity operates in the linear region as depicted in Fig. 2. In the rest of this paper, we present the design and experimental implementation of an integral LQG controller as an example implementation of the various quantum control techniques that could be applied to the optical cavity controller test bed system.

### III. EXAMPLE APPLICATION OF A SYSTEMATIC CONTROL TECHNIQUE ON THE TEST BED

This section describes the application of an integral LQG controller as an example application of a systematic modern control scheme for locking the three-mirror ring cavity on the optical test bed. Here, we describe the method used to model the plant, design an integral LQG controller using this model, and provide details of the experimental implementation and closed-loop performance of the controller.

### A. Modeling the Cavity and Piezoelectric Actuator Dynamics: System Identification

As a first step in designing an integral LQG controller for locking the optical cavity, we identify a model describing the dynamics of the cavity and the PZT actuator. In order to obtain a plant model that includes the dynamics of the cavity as well as the PZT actuator, frequency response data for the plant, which consists of the cavity and the PZT actuator, is recorded using an HP 35665A 2-channel DSA.

The setup used for recording the frequency response data for the plant is depicted in Fig. 3. The cavity is held in lock using a suitable analog PI controller during the process of data acquisition. A swept sinusoidal signal generated by the DSA (denoted  $\mathbf{R}$  in Fig. 3) is applied to the closed-loop system as shown in Fig. 3. The DSA then produces the frequency response corresponding to the quantity  $Y(j\omega)/U(j\omega)$ , which is the required frequency response for the plant. For a physical interpretation of the signals  $Y(j\omega)$  and  $U(j\omega)$ , consider the quantum optical model defined in (1). We can linearize (1) about the expected values of each of the parameters in the equations and solve them in the Fourier transform domain. When the cavity is locked to  $\langle \Delta \rangle = \bar{\Delta} = 0$ , the Fourier-domain amplitude and phase quadratures of the cavity are

$$\begin{aligned} \delta\tilde{X}_r^\pm(j\omega) &= \frac{2\kappa_1 - \kappa - j\omega}{\kappa + j\omega} \delta\tilde{X}_{in}^\pm(j\omega) + \frac{2\sqrt{\kappa_1\kappa_2}}{\kappa + j\omega} \delta\tilde{X}_v^\pm(j\omega) \\ &\quad + \frac{2\sqrt{\kappa_1\kappa_3}}{\kappa + j\omega} \delta\tilde{X}_l^\pm \mp \frac{2\kappa_1 X_{in}^\mp}{\kappa(\kappa + j\omega)} \delta\tilde{\Delta}(j\omega). \end{aligned} \quad (3)$$

As discussed previously, the frequency detuning  $\Delta$  is related to the position of mirror M3 relative to the position at resonance. The position of the mirror M3 is itself determined by the dynamics of the mirror, PZT to which the mirror is attached, mirror mount to which the PZT is attached, and HV AMP that drives the PZT. In the Fourier domain, we can define a lumped classical transfer function  $G_C(j\omega)$  from the voltage applied to the HV AMP  $U(j\omega)$  to the position of the mirror  $\delta\tilde{\Delta}(j\omega)$ . Making use of our simplification that  $X_{in}^- = 0$ , the transfer function definition for  $G_C(j\omega)$ , and the fact that the input field is much greater than the vacuum fields incident on mirrors M2 and M3, we have  $X_{in}^+ \delta\tilde{\Delta}(j\omega)/\kappa \gg \delta\tilde{X}_{in}^-(j\omega), \delta\tilde{X}_v^-(j\omega), \delta\tilde{X}_l^-(j\omega)$ . Hence, (3) can be rewritten as

$$\begin{aligned} \delta\tilde{X}_r^-(j\omega) &\approx \frac{2\kappa_1 X_{in}^+}{\kappa(\kappa + j\omega)} G_C(j\omega) U(j\omega) \\ &= G_Q(j\omega) G_C(j\omega) U(j\omega) \\ &= G(j\omega) U(j\omega). \end{aligned} \quad (4)$$

In (4), we have defined a quantum transfer function  $G_Q(j\omega) = 2\kappa_1 X_{in}^+/\kappa(\kappa + j\omega)$ , which models the dynamics of the quantum optical cavity. The full transfer function of the entire system is thus the product of the classical and quantum dynamics of the system, being  $G(j\omega) = G_Q(j\omega) G_C(j\omega)$ . Finally, we treat the phase quadrature homodyne measurement of the quantum optical field reflected from the cavity as being the measurement input to a controller,  $Y(j\omega)$ . Then, we can

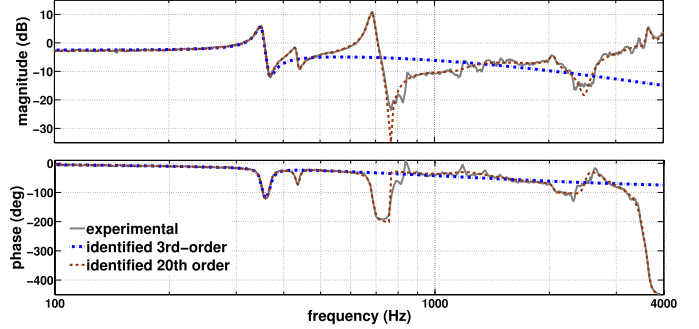


Fig. 4. Plant frequency response comparison of experimental data obtained from the DSA, 20th-order identified model, and third-order identified model.

see that the transfer function for the combined quantum-classical plant is easily measured to be  $Y(j\omega)/U(j\omega)$ . Both quantities,  $U(\cdot)$  and  $Y(\cdot)$  are measured in volts.

The gain and phase of the experimentally measured data is plotted in Fig. 4. For the purpose of controller design, we consider the frequency response data up to the first resonance. This is justified by the fact that it is usually only necessary to suppress the first resonant mode in the system, which is the primary mode of the cavity and contributes most to the dynamics of the cavity [30], [31]. This data corresponds to the frequency response data between 100 and 400 Hz in Fig. 4. The iterative PEM method from the system identification toolbox in MATLAB was used in order to fit a third-order model to the truncated frequency response data and a 20th order model for the full response. The third-order model will be used for control system design and the 20th-order model will be used for simulation purposes in Section III-C. A comparison of the three frequency responses is shown in Fig. 4.

The third-order model for the plant was a state space model of the form

$$\dot{x}(t) = Ax(t) + Bu(t); \quad z(t) = Cx(t) + Du(t) \quad (5)$$

where

$$\begin{aligned} A &= 10^4 \times \begin{bmatrix} -0.0180 & -0.2865 & 0.0573 \\ 0.1693 & -0.0157 & 0.2339 \\ 0.0446 & 0.1109 & -1.1449 \end{bmatrix} \\ B &= \begin{bmatrix} 2.8394 \\ 4.2852 \\ -24.9287 \end{bmatrix}^T \\ C &= \begin{bmatrix} 24.0014 \\ 37.3086 \\ -34.4903 \end{bmatrix}^T \\ D &= 0. \end{aligned} \quad (6)$$

Here,  $x \in \mathbb{R}^3$  is the state vector,  $u \in \mathbb{R}$  is the input, and  $z \in \mathbb{R}$  is the output.

### B. Integral LQG Controller Design

As outlined in Section II, the control objective is to drive the error signal (output of the HD) to zero in order to achieve

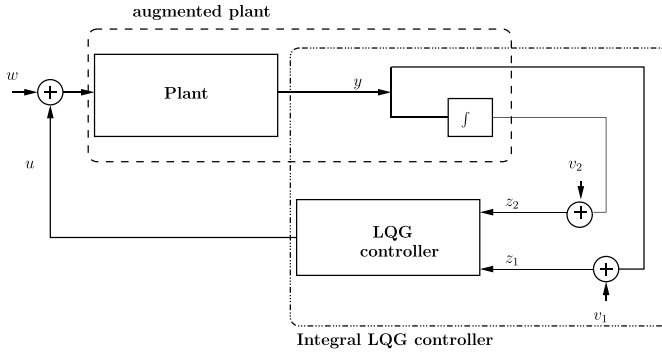


Fig. 5. Plant output augmented with an integrator to overcome slowly varying drifts and offsets.

cavity locking, while maintaining the transmitted signal (output at mirror M2) at maximum. In the ideal case, a simple LQG controller would suffice in achieving this control objective, but since the cavity is subjected to slowly varying drifts and offsets, these effects need to be considered while designing the controller. In order to address these issues, the plant is augmented with an integrator, which provides rejection of low-frequency disturbances, reduces the overall sensitivity to model errors at lower frequencies, and provides robust closed-loop performance in the presence of drift in the homodyne error signals. This augmented plant is then considered in designing the integral LQG controller, with two inputs and one output as depicted in Fig. 5.

The dynamics of the augmented plant is given by

$$\dot{x}_a = A_a x_a + B_a u + B_a w \quad (7)$$

$$z_a = C_a x_a + v \quad (8)$$

where  $v = [v_1 \ v_2]^T$ ,  $x_a = [x \ \int y dt]^T$  is the augmented state vector with  $x_a \in \mathbb{R}^4$ , and  $z_a = [z_1 \ z_2]^T$  is the augmented output vector. In addition, the matrices for the augmented system are defined as

$$A_a = \begin{bmatrix} A & 0 \\ C & 0 \end{bmatrix}, \quad B_a = \begin{bmatrix} B \\ 0 \end{bmatrix}, \quad C_a = \begin{bmatrix} C & 0 \\ 0 & I \end{bmatrix} \quad (9)$$

where  $x$ ,  $A$ ,  $B$ , and  $C$  are defined in (5) and (6).

For the augmented plant outlined in (7)–(9), the integral LQG controller is designed by minimizing a quadratic cost function of the form

$$\mathfrak{J} = \lim_{t_f \rightarrow \infty} \mathbb{E} \left[ \frac{1}{t_f} \int_0^{t_f} \left( x^T Q x + f(y)^T Q_I f(y) + u^T R u \right) dt \right] \quad (10)$$

where  $f(y) = \int_0^{t_f} y(\tau) d\tau$ ,  $\mathbb{E}[\cdot]$  is the expected value, and  $t_f$  is the final time. In addition,  $Q \geq 0$ ,  $Q_I \geq 0$ , and  $R > 0$  are weighting matrices associated with the state, integral state, and control input, respectively. The error signal  $y(t)$  in Fig. 5 is measured using the homodyne measurement method described in Section II and is proportional to the amount of detuning in the system. The control objective in the design of the integral LQG controller is to reduce this error signal to zero so as to achieve cavity

locking. The integral LQG controller is described by the equations

$$\dot{\hat{x}}_a = A_a \hat{x}_a + B_a u + K(z_a - C_a \hat{x}_a); \quad u = -L \hat{x}_a. \quad (11)$$

Here,  $\hat{x}_a$  is the estimated augmented state vector obtained from a steady-state Kalman filter and  $K$  is the associated Kalman gain defined as  $K = P_K C_a^T R_K^{-1}$ , where  $P_K \geq 0$  is the solution to the algebraic Riccati equation

$$A_a P_K + P_K A_a^T - P_K C_a^T R_K^{-1} C_a P_K + Q_K = 0. \quad (12)$$

Here,  $Q_K \geq 0$  and  $R_K > 0$  are the process and measurement noise variances defined, respectively, as  $Q_K = \sigma_1^2$ ,  $R_K = \text{diag}(\sigma_2^2, \sigma_3^2)$ , where  $\text{diag}(\cdot)$  denotes the diagonal matrix with given entries in the diagonal. In addition,  $\sigma_1$  is the standard deviation associated with the process noise  $w_1$ ,  $\sigma_2$  is the standard deviation associated with the measurement noise  $v_1$  of the HD, and  $\sigma_3$  is the standard deviation associated with the measurement noise  $v_2$  of the augmented integral output signal.

The feedback gain matrix  $L$  in (11) is given by

$$L = R_C^{-1} B_a P_C \quad (13)$$

where  $P_C \geq 0$  is the solution to the algebraic Riccati equation

$$A_a P_C + P_C A_a^T - P_C C_a^T R_K^{-1} C_a P_C + Q_C = 0 \quad (14)$$

with the controller weighting matrix  $R_C = r$  and  $Q_C = C_a^T \text{diag}(1, q) C_a$ . Here,  $q$  is the weighting on the integral term and  $r$  is the weighting on the control term in the LQG cost function (10). The various parameter values chosen in the design process for the integral LQG controller were: 1)  $\sigma_1^2 = 1$ ; 2)  $\sigma_2^2 = 1$ ; 3)  $\sigma_3^2 = 10^{-7}$ ; 4)  $q = 5 \times 10^5$ ; and 5)  $r = 0.5$ . According to a standard method for designing practical LQG controllers, these noise covariances and weighting parameters were considered to be design parameters and need not necessarily reflect the actual covariances in the system [34]. The value for  $\sigma_1$  was normalized to one, whereas the values for  $\sigma_2$  and  $\sigma_3$ , corresponding to measurement noise sources, were chosen to provide a suitable bandwidth for the LQG controller [34]. Similarly, the cost weighting parameters  $q$  and  $r$  in the design of the LQG controller state feedback gain were chosen to obtain acceptable values for the gain crossover frequency, gain margin, and phase margin of the loop-gain corresponding to the product of the augmented plant transfer function and integral LQG controller transfer function [34]–[36]. The frequency response for the corresponding loop-gain transfer function is shown in Fig. 6, which has a gain margin of 20.2 dB at 251 Hz, phase margin of 47° at 61 Hz, and gain crossover frequency of 61 Hz. These robustness margin values were chosen in order to ensure closed-loop stability of the control system before implementing the controller on the optical test bed system. Such a check is necessary to guarantee adequate robustness margins for LQG controllers as suggested in [37]. Note that the magnitude of the loop-gain rolls off at higher frequencies beyond those shown in Fig. 6.

The state space model for the integral LQG controller was discretized before implementing it, using the dSPACE DSP

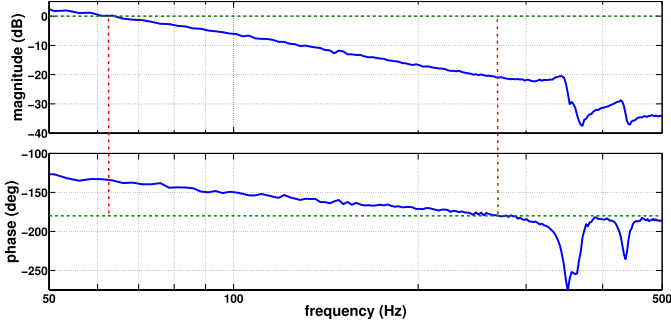


Fig. 6. Bode plot of the loop-gain corresponding to the experimental plant data and the integral LQG controller.

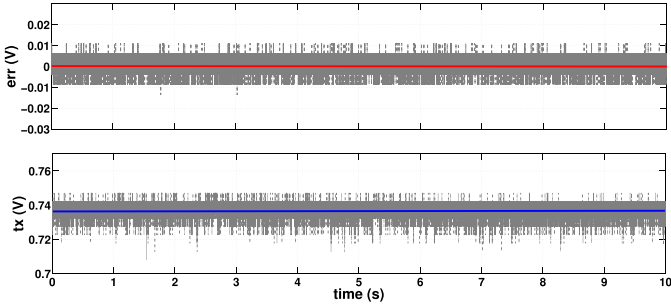


Fig. 7. Experimentally measured error signal and transmitted signal using the integral LQG controller. The mean values for the error signal and the transmitted signal are depicted by solid lines, which are 0 V and 0.738 V respectively.

system. For a detailed discussion on the LQG controller design process for practical applications, including choosing noise covariances for the design of Kalman filters and weighting matrices for the LQG cost function, see [34]–[36].

As mentioned in Section I, PID controllers have been traditionally used for locking optical cavities [10]. They are classical controllers of order two (when a finite bandwidth version is considered), whereas the current LQG controller implemented in this paper is a fourth-order controller as dictated by the system model order. Hence, the LQG controller design considered in this case, offers more flexibility, leading to better closed-loop performance, than a PID controller. Although both methods involve choosing of design parameters, the parameter values have a more direct interpretation in the LQG design than in a PID design. In addition, for a given set of noise covariances and weighting matrices, the LQG controller is an optimal controller [34].

### C. Controller Implementation and Experimental Results

A schematic view with a detailed description of the various components used in experimentally frequency locking the ring cavity in the optical controller test bed system was described in Section II. The analog error signal obtained from the output of mirror M1 via the process of homodyne detection is converted into a digital form using a 12-bit analog-to-digital converter (ADC) on a DS1104 dSPACE DSP system. This digital error signal is split into two signals: 1) original error signal (denoted  $y$  in Fig. 5) and 2) synthesized signal comprising of an integral of the error signal. These two signals are used as inputs by the integral LQG controller to

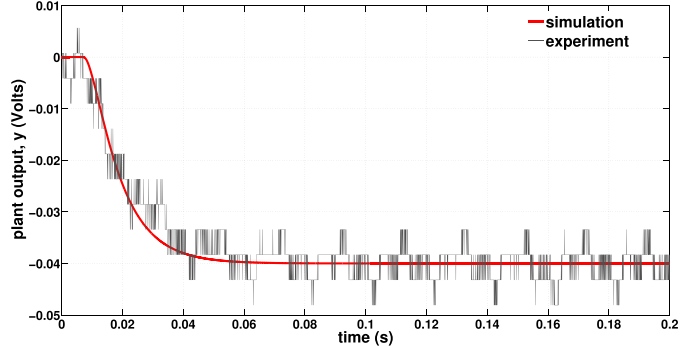


Fig. 8. Comparison of closed-loop step response: experiment versus simulation.

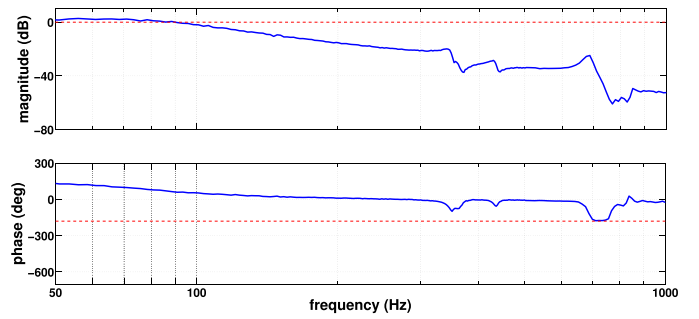


Fig. 9. Closed-loop frequency response.

provide a suitable control signal. The resulting digital control signal is fed to a digital-to-analog converter on the dSPACE system and the corresponding analog signal is amplified using a high voltage amplifier (HV AMP) before being applied to the PZT actuator mounted on mirror M3. The amplitude of the control signal applied to the PZT actuator dictates the amount by which mirror M3 is moved, hence altering the resonant frequency of the cavity.

A plot of the error signal (output of the homodyne detector) and transmitted signal (output at mirror M2 or the transmitted port) in lock using the integral LQG controller is shown in Fig. 7. As can be seen from the plots in Fig. 7, the error signal is held close to zero and the transmitted signal is held close to a maximum value of  $\approx 0.738$  V, satisfying the control objectives outlined in Section II.

The performance of the closed-loop system with the integral LQG controller was evaluated by considering its closed-loop step response in both the experiment as well as in simulation. Here, the third-order plant model in Fig. 4 was used to design the controller for experimental implementation using the dSPACE DSP board. In the case of the simulation, the complete frequency response data for the frequency range 10–5000 Hz was considered in modeling the dynamics for the plant. This was achieved by fitting a 20th-order model to the frequency response data in the frequency range 10–5000 Hz using the PEM method. The results were depicted in Fig. 4. The step responses obtained experimentally and in simulation are compared in Fig. 8 and the corresponding closed-loop frequency response is shown in Fig. 9. A step input of 0.04 V was used to test the performance of the integral LQG controller both in the experiment as well as simulation. The output

of the plant  $y$ , which is at 0 V initially, responds to this change and settles within 0.1 s to a mean value of  $-0.0391$  V. The performance of the closed-loop system was found to be stable over all operational conditions and the controller was successful in maintaining cavity lock over extended periods of time. This provides an experimental demonstration of the robustness of the designed integral LQG controller. The observed noise in the experimental step response is mainly due to the quantization effects arising from the use of the 12-bit ADC on the DS1104 dSPACE DSP board. These quantization errors in Figs. 7 and 8 are consistent with the errors introduced by the 12-bit ADC and represent the dynamic range of the DSP board. Furthermore, scaling of the signals might improve the effects of quantization error on the step response at the expense of saturation of the signal supplied to the controller, due to large and time-varying offsets.

#### IV. CONCLUSION

This paper described a test bed system for implementing and testing systematic modern control techniques used in frequency locking optical cavities. The optical cavity test bed system comprised of an input laser, a three-mirror ring cavity, the associated optics, and a dSPACE DSP system. The dynamics of the plant comprising of the three-mirror ring cavity and the PZT actuator system were obtained from frequency response data recorded using a DSA. A third-order model was fitted to the truncated frequency response data up to the first system resonance and was augmented with an integrator. The augmented plant model was used to design an integral LQG controller in order to achieve frequency locking for the optical cavity. The controller was discretized and implemented using a dSPACE DSP system. It was noted that the controller satisfied the control objectives, namely, regulating the detuning parameter to zero while maximizing the transmitted signal. The stability and robustness of the closed-loop system was verified experimentally by measuring its step response and comparing it with the step response obtained in simulation.

#### REFERENCES

- [1] A. Abramovici *et al.*, "LIGO: The laser interferometer gravitational-wave observatory," *Science*, vol. 256, no. 5055, pp. 325–333, Apr. 1992.
- [2] C. Y. Lee, C. Zhao, E. J. Chin, J. Jacob, D. Li, and D. G. Blair, "Control of pre-isolators for gravitational wave detection," *Classical Quantum Gravity*, vol. 21, no. 5, p. S1015, Feb. 2004.
- [3] B. Dahmani, L. Hollberg, and R. Drullinger, "Frequency stabilization of semiconductor lasers by resonant optical feedback," *Opt. Lett.*, vol. 12, no. 11, pp. 876–878, Nov. 1987.
- [4] B. A. Paldus *et al.*, "Cavity-locked ring-down spectroscopy," *J. Appl. Phys.*, vol. 83, no. 8, pp. 3991–3997, Apr. 1998.
- [5] A. G. Kallapur, T. K. Boyson, I. R. Petersen, and C. C. Harb, "Nonlinear estimation of ring-down time for a Fabry-Perot optical cavity," *Opt. Exp.*, vol. 19, no. 7, pp. 6377–6386, Mar. 2011.
- [6] H. Mabuchi and A. C. Doherty, "Cavity quantum electrodynamics: Coherence in context," *Science*, vol. 298, no. 5597, pp. 1372–1377, Nov. 2002.
- [7] K. J. Vahala, "Optical microcavities," *Nature*, vol. 424, no. 6950, pp. 839–846, 2003.
- [8] J. Klaers, J. Schmitt, F. Vewinger, and M. Weitz, "Bose-Einstein condensation of photons in an optical microcavity," *Nature*, vol. 468, no. 7323, pp. 545–548, Nov. 2010.
- [9] J. Ye and T. W. Lynn, *Applications of Optical Cavities in Modern Atomic, Molecular, and Optical Physics* (Advances In Atomic, Molecular, and Optical Physics), vol. 49. San Diego, CA, USA: Academic, 2003, pp. 1–83.
- [10] C. C. Harb, "Stabilization of a ring dye laser," M.S. thesis, Dept. Quantum Sci., Australian Nat. Univ., Canberra, Australia, 1992.
- [11] D. A. Shaddock, M. B. Gray, and D. E. McClelland, "Frequency locking a laser to an optical cavity by use of spatial mode interference," *Opt. Lett.*, vol. 24, no. 21, pp. 1499–1501, Nov. 1999.
- [12] J. L. Thorpe, K. Numata, and J. Livas, "Laser frequency stabilization and control through offset sideband locking to optical cavities," *Opt. Exp.*, vol. 16, no. 20, pp. 15980–15990, Sep. 2008.
- [13] Q.-F. Chen, A. Neovsky, and S. Schiller, "Locking the frequency of lasers to an optical cavity at the  $1.6 \times 10^{-17}$  relative instability level," *Appl. Phys. B*, vol. 107, no. 3, pp. 679–683, Jun. 2012.
- [14] A. C. Doherty and K. Jacobs, "Feedback-control of quantum systems using continuous state-estimation," *Phys. Rev. A*, vol. 60, no. 4, pp. 2700–2711, Oct. 1999.
- [15] S. C. Edwards and V. P. Belavkin, "Optimal quantum feedback control via quantum dynamic programming," School of Math. Sci., Univ. Nottingham, Nottingham, U.K., Tech. Rep. quant-ph/0506018, Jun. 2005.
- [16] M. R. James, H. I. Nurdin, and I. R. Petersen, " $H^\infty$  control of linear quantum stochastic systems," *IEEE Trans. Autom. Control*, vol. 53, no. 8, pp. 1787–1803, Sep. 2008.
- [17] G. J. Milburn, "Decoherence and the conditions for the classical control of quantum systems," *Philosoph. Trans. Roy. Soc. A*, vol. 370, no. 1975, pp. 4469–4486, Sep. 2012.
- [18] B. Willke *et al.*, "Spatial and temporal filtering of a 10-W Nd:YAG laser with a Fabry-Perot ring-cavity premode cleaner," *Opt. Lett.*, vol. 23, no. 21, pp. 1704–1706, Nov. 1998.
- [19] S. Z. S. Hassen, M. Heurs, E. H. Huntington, I. R. Petersen, and M. R. James, "Frequency locking of an optical cavity using linear quadratic Gaussian integral control," *J. Phys. B, Atomic, Molecular Opt. Phys.*, vol. 42, no. 17, p. 175501, Aug. 2009.
- [20] M. Heurs, I. R. Petersen, M. R. James, and E. H. Huntington, "Homo-dyne locking of a squeezer," *Opt. Lett.*, vol. 34, no. 16, pp. 2465–2467, Aug. 2009.
- [21] R. L. Barger, M. S. Sorem, and J. L. Hall, "Frequency stabilization of a CW dye laser," *Appl. Phys. Lett.*, vol. 22, no. 11, pp. 573–575, Mar. 1973.
- [22] A. D. White, "Frequency stabilization of gas lasers," *IEEE J. Quantum Electron.*, vol. 1, no. 8, pp. 349–357, Nov. 1965.
- [23] D. Hils and J. L. Hall, "Response of a Fabry-Perot cavity to phase modulated light," *Rev. Sci. Instrum.*, vol. 58, no. 27, pp. 1406–1412, Apr. 1987.
- [24] R. V. Pound, "Electronic frequency stabilization of microwave oscillators," *Rev. Sci. Instrum.*, vol. 17, no. 11, pp. 490–505, Dec. 1946.
- [25] R. W. P. Drever *et al.*, "Laser phase and frequency stabilization using an optical resonator," *Appl. Phys. B, Lasers Opt.*, vol. 31, no. 2, pp. 97–105, Jun. 1983.
- [26] T. W. Hensch and B. Couillaud, "Laser frequency stabilization by polarization spectroscopy of a reflecting reference cavity," *Opt. Commun.*, vol. 35, no. 3, pp. 441–444, Dec. 1980.
- [27] C. W. Gardiner and P. Zoller, *Quantum Noise*. Berlin, Germany: Springer-Verlag, 2000.
- [28] H. A. Bachor and T. C. Ralph, *A Guide to Experiments in Quantum Optics*. New York, NY, USA: Wiley, 2004.
- [29] L. Ljung. (2002, Jan./Feb.). "Prediction error estimation methods," *Circuits, Syst. Signal Process.* [Online]. 21(1), pp. 11–21. Available: <http://dx.doi.org/10.1007/BF01211648>
- [30] S. S. Aphale, S. O. R. Moheimani, and A. J. Fleming, "Dominant resonant mode damping of a piezoelectric tube nanopositioner using optimal sensorless shunts," in *Proc. Amer. Control Conf. (ACC)*, New York, NY, USA, 2007, pp. 2220–2225.
- [31] S. S. Aphale, A. J. Fleming, and S. O. R. Moheimani, "Integral resonant control of collocated smart structures," *Smart Mater. Struct.*, vol. 16, no. 2, pp. 439–446, Feb. 2007.
- [32] A. G. Kallapur *et al.*, "Digital locking of a three-mirror ring cavity," in *Proc. IEEE Int. Conf. Control Appl. (CCA)*, Dubrovnik, Croatia, Oct. 2012, pp. 75–79.
- [33] G. N. Milford, C. C. Harb, and E. H. Huntington, "Shot noise limited, microwave bandwidth photodetector design," *Rev. Sci. Instrum.*, vol. 77, no. 11, pp. 114701-1–114701-6, Nov. 2006.
- [34] J. P. Hespanha, *Linear Systems Theory*, 23rd ed. Princeton, NJ, USA: Princeton Univ. Press, 2009.
- [35] T. Glad and L. Ljung, *Control Theory*. New York, NY, USA: Taylor & Francis, 2000.
- [36] H. Richter, *Advanced Control of Turbofan Engines*. New York, NY, USA: Springer-Verlag, 2012.
- [37] J. Doyle, "Guaranteed margins for LQG regulators," *IEEE Trans. Autom. Control*, vol. 23, no. 4, pp. 756–757, Aug. 1978.